Received: 30 October 2019 | Revised: 15 January 2020 | Accepted: 27 January 2020

DOI: 10.1111/ijag.15107

SPECIAL ISSUE ARTICLE

INTERNATIONAL JOURNAL OF Applied Glass SCIENCE

Processing technologies for sealing glasses and glass-ceramics

Araceli de Pablos-Martín[1] | **Sonia Rodríguez-López**[2] | **Maria J. Pascual**[2]

[1]Fraunhofer Institute for Microstructure of Materials and Systems IMWS, Halle, Germany

[2]Ceramics and Glass Institute (CSIC), Madrid, Spain

Correspondence
Araceli de Pablos-Martin, Fraunhofer Institute for Microstructure of Materials and Systems IMWS, Walter-Huelse-Strasse 1, 06120 Halle, Germany.
Email: araceli.pablos-martin@imws.fraunhofer.de

Funding information
FP7 Joint Technology Initiatives, Grant/Award Number: 278525; Conselho Nacional de Desenvolvimento Científico e Tecnológico, Grant/Award Number: 400590/2013; FhG Internal Programs, Grant/Award Number: Attract 692 280

Abstract

This paper embraces two different approaches for the joining of materials through glass sealants. First, the conventional method of furnace sealing in which paste technology is normally employed. The glass sealant is applied in powder form mixed with agglomerant and with the help of dispenser robots, tape casting, or screen printing. Glass-ceramics for sealing of solid oxide fuel cells (SOFC) are described as an example of this type of processing. Glass composition, thermal properties, particle size of the glass powder, sintering and crystallization competition, and final crystalline phases together with a suitable chemical compatibility with the metallic and ceramic elements to be sealed need to be carefully adjusted for this specific application. Second, laser welding is presented as an alternative sealing technology. A general overview about laser welding through glass sealants is presented. Particularly, the welding of sapphire and fused silica glass through a BTS.2SiO_2 thin film glass sealant by employment of a nanosecond-pulsed laser is detailed. Laser parameters (frequency, power, scan speed, and number of passes) were optimized to get the best molten conditions of the BTS thin film, while allowing its crystallization. BTS crystallization upon laser welding leads to a strong blue emission upon UV excitation. Finally, both processing technologies were compared.

KEYWORDS

adherence, crystallization, fresnoite, furnace sealing, glass-ceramics, laser welding, sintering

1 | INTRODUCTION

The term sealing glass, more than a composition or specific property, describes the use of glass to create a hermetic seal. Glasses are known from the antiquity but the use of glass with the purpose of obtaining hermetic seals is relatively recent and its development is linked to the growing of the electronic and semiconductors industry.

The joining glass/metal or glass/ceramic is a field or research which covers the fields of energy generation systems, electricity, microelectronics, and protection against corrosion. The study of the sealing glasses implies an interdisciplinary research and development work connecting different areas of knowledge such as the design and preparation of glass compositions, adherence, and interdiffusion processes and also the most modern techniques for the study of surfaces and interfacial reactions.

The glass properties must be adjusted to strict certain values in order to be used in a particular system. The specifications that the glass must fulfil to be effective as a sealing material depend on the nature of the materials to be sealed, the complexity of the system, the different functionalities that the seal must perform, and the system working conditions.[1] In many of the applications, the glass sealant will not only carry out the sealing function but also others such as electrical isolator, environmental protection, chemical and mechanical protection, diffusional barrier, etc.

In particular, the manufacturing of SOFC stacks requires a joining process to obtain a gastight and electrically insulating joint between generally two metallic parts (window frame and interconnect) and to separate cathode and anode in an anode-supported p-SOFC in order to stack a serial repeat unit. The most common materials employed for this application are glass-ceramic (GC) sealants because of their good mechanical and electrical insulation properties and the possibility to use a wide range of chemical compositions to control some of its properties. Generally, for sealing, a paste obtained from glass powder mixed with alcohol and a binder is prepared and applied to the parts to be sealed; after that, the entire stack is heated up at temperatures between 800°C and1000°C in an electrical furnace for few hours.[2,3] Normally, the application of the glass powder takes place with the help of dispenser robots, tape casting, or screen printing.[4] This is a typical example of conventional furnace sealing. In this case, glass composition, thermal properties, particle size of the glass powder, sintering and crystallization competition, and final crystalline phases together with a suitable chemical compatibility with the metallic and ceramic elements to be sealed need to be carefully adjusted.

An alternative to the conventional sealing process is the laser welding. This technique offers the advantages of the application of precise and focused energy (without the need of heating the complete system) due to the high-power density of the laser. The basic principle of the laser welding technique is the melting of the material in the interphase in contact with the joint partners through the energy of the laser beam.[5]

For the optimization of the laser welding parameters, the optical and thermal properties, such as optical transmission, optical penetration depth and index of refraction at the laser wavelength, heat conduction, melting point, and coefficient of thermal expansion (CTE) of the materials to be welded and that of the sealant are key not only to achieve a good weld, but also to understand the weld process.

For laser welding process, the glass sealant is usually milled to some microns of grain size and applied as a paste forming a layer to the joint surface. Heat accumulation is crucial, since the glass sealant must be molten, while the joint substrates have to remain undamaged under the high temperature reached. Thereof, high repetition rates and low scan speeds are preferred upon the adequate laser power. Several scan passes and *wobbling* can be very useful, as well.[6] There are mainly two joint configurations: (a) Direct coupling: The beam is coupled directly into the glass sealant. Here a CO_2 laser is usually employed, since at the wavelength of 10.6 μm the radiation is mostly absorbed by the glass sealant[7]; (b) Laser transmission bonding (LTB): Here the *sandwich* substrate/sealant/substrate is perpendicular to the laser beam, with the upper substrate facing the laser beam. For transparent (to the laser wavelength) substrates, the laser beam goes through the upper substrate and is focused directly on the glass sealant (or on the absorbing lower substrate), depositing the energy in the joining area. In this configuration, visible to near-infrared pulsed lasers can be focused in the interior of beneath the substrates, without affecting their surfaces.[6]

In the literature, it is surprising the lack of works focused on the laser-assisted sealing through glass sealants, in comparison with those reporting on the conventional furnace sealing. Some examples of laser welded substrates through glass sealants are summarized in Table 1. Substrates of different chemical nature (metals, glasses, ceramics) were joined through glass sealants

TABLE 1 Data of selected publications on laser sealing through glass sealants

Joint substrates	Glass sealant system	Laser, wavelength (nm)	Power (W)	Processing speed	Reference
ZrO_2/ZrO_2	SiO_2–BaO–B_2O_3, BaO–SrO–SiO_2	808 940	170-330	500 mm/s	(11)
Na, Ca-based Glass/ SnO_2:F-coated Glass	Pb-free Glass frit	Yb-fiber diode laser	44	400 mm/s	(9)
Crofer22APU	SiO_2–BaO–CaO	Nd:YAG, 1064 nm, pulsed CO_2, 10 600 nm, CW Diode, 808 940, CW	220 6000 1000	Static. Processing time: 120 s	(7)
Crofer22APU	SiO_2–BaO–MgO–B_2O_3	CO_2, 10 600 nm, CW	90	Laser *cladding*. 10 mg/s glass sealant paste	(8)
Alumina/sapphire	CaO–Al_2O_3–SiO_2	CO_2, 10 600 nm, CW	n.r (corresponding to 990°C)	n.r	(10)
SiC/SiC	Y_2O_3–Al_2O_3–SiO_2	Diode laser, 808 940, CW	875-1230 W/cm^2	Irradiation time: 70 s	(13)
Na_2O–CaO–MgO–SiO_2–based glasses	V_2O_5–TeO_2– BaO–ZnO–B_2O_3	Diode laser, 810 nm	40	300 mm/s 200 irradiation cycles	(12)

Abbreviation: CW, Continuous wave, n.r: not reported.

Note: Glass sealants were prepared by melting and quenching process and the glass coatings were achieved by screen-printing-based technique.

by this technique.[7–13] Some of these laser welded joints are employed to seal solar cells.[9,14–17]

In our work, we selected fresnoite (BTS) glasses as sealants for transparent materials. BTS glasses of composition $2BaO–TiO_2–2SiO_2$ and its derivatives (eg, $2SrO–TiO_2–2SiO_2$ and $2BaO–TiO_2–2GeO_2$) are very well-known and still under study, due to its unique properties.[18] The Ti^{4+} ions in fivefold coordination leads to a characteristic fluorescence in the blue region of the spectrum upon excitation in the UV range, which is more intense in the BTS crystal than in the parent glass. Thus, the crystallization of BTS has been exhaustively studied, including laser crystallization of BTS bulk glasses[19–21] and BTS thin films.[22] Laser irradiation induces the local crystallization of BTS, and the subsequent blue luminescence of the irradiated sites upon UV excitation. This was our main motivation for the use of BTS as a glass sealant, since the idea of a luminescent glass sealant is very attractive in the fields of optics and micro electromechanical systems (MEMS). Furthermore, BTS is known to crystallize very rapidly in comparison with other silicate glasses.[23]

In our previous works, different combinations of transparent materials and BTS-based thin films acting as sealants were investigated.[24–28] One of the novelties of those works was that the BTS glass sealant was employed as thin film (1-2 μm thickness) obtained from Pulsed Laser Deposition (PLD) process, and not as paste from glass powders (Table 1). In Ref. (26), we reported on the laser welding of two transparent dissimilar substrates, being sapphire and fused silica. Both materials are extensively used in the fields of optics and MEMS. The glass sealant employed was a nonstoichiometric BTS thin film, enriched in SiO_2, of composition $BTS.3SiO_2$. By increasing the SiO_2 content, the difference between the coefficients of thermal expansions (CTE) of the substrates (saphire and fused silica) and the thin filmsealant (BTS) decreases.

In the following two concrete examples of both processing technologies are presented. The first example is focused on glass-ceramic sealants for SOFC in which the conventional furnace sealing is applied explaining how the glass composition can be adjusted to fulfill the specific requirements for this application together with the determination of dilatometric properties and sintering behavior to select the most suitable compositions. Finally, stable joints of steel/glass-ceramic/half-cell are obtained by heating in a furnace according to the typical heating schedule of a SOFC stack. The second example is focused on the laser welding of fused silica and sapphire through a $BTS.2SiO_2$ glass thin film. Additional results of the previous $BTS.3SiO_2$ glass sealant are shown for comparison, as well. The results aim to consolidate the feasibility of the employment of BTS-based thin film glass sealants for the welding of transparent dissimilar substrates, by using a nanosecond pulsed laser, different to the lasers conventionally used (Table 1).

2 | EXPERIMENTAL PROCEDURE

2.1 | Sealing glass-ceramics for SOFC—Paste technology and conventional furnace sealing

Glass compositions within the system $BaO/SrO–MgO/ZnO–B_2O_3–SiO_2$ were designed and studied in this work. The raw materials used for the preparation of the glasses were: silica sand (99.6%), $BaCO_3$ (Alfa Aesar, 99.8%), $SrCO_3$ (Alfa Aesar, 97.5%), MgO (Panreac, 98.0%), ZnO (Panreac, 99.0%), and vitreous B_2O_3. The B_2O_3 powders (Alfa Aesar, 99.0%) were melted first in a gas furnace at 900ºC to obtain a glass, thus avoiding the hygroscopic character of the B_2O_3 powders. The glass components were mixed in a mixer (Turbula, mixer, WAB) for 1 hour before calcination was carried out at 1250ºC–1300ºC in an electrical furnace using a covered Pt/Rh crucible with subsequent melting at 1550ºC for 2 hours. The batch was melted twice to ensure proper glass homogeneity. The molten glass was poured into brass molds to get bulk glass samples and also in water to get glass frits. The glass frits were dried at 100ºC and milled in a planetary mill using an agate mortar and sieved to obtain a fraction of powders <63 μm to study samples by hot-stage microscopy (HSM).

The dilatometric properties of bulk glass pieces (glass transition temperature T_g, dilatometric softening temperature T_d, and thermal expansion coefficient (TEC)) were measured by a Netzsch Gerätebau 402 EP dilatometer equipped with a silica support.

Hot-stage microscopy was performed using a LeicaEM201 microscope (Leica Microsystems GmbH, Wetzlar, Germany) with image analysis (Hesse Instruments) for determination of the sintering and fluency of glass powders in air at a heating rate of 2 K/min up to 1000ºC. The glass powder samples were initially cold-pressed to conformed bodies of 3 mm in both height and diameter. The temperature was measured with a Pt/Rh (6130) thermocouple (Type B, Heraeus) placed under and in contact with the substrate. Pieces of Crofer22APU were used as substrates in order to see if bonding takes place.

Joints of the type steel/glass-ceramic/half-cell were prepared using Crofer22APU and Crofer22H. The glass is applied as a paste after mixing the glass powders with ethanol. A typical thermal treatment up to 850ºC for 10 hours was used with a heating rate of 2 K/min, simulating the start-up an operation of a SOFC.

The microstructure of the obtained glass-ceramic joints was observed using a field emission scanning electron microscope FE-SEM model Mira3 (Tescan) with a coupled X-ray fluorescence spectrometer for the dispersive energy (EDX) Silicon Drift Detector (SDD)-XMaxN, Oxford Instruments.

2.2 | Laser sealing of fused silica with sapphire through a BTS·2SiO_2 glass thin film

For the laser welding processing, a BTS glass with an excess of SiO_2 of nominal composition 2BaO–TiO_2–4SiO_2, from now on as BTS.2SiO_2, was prepared using the conventional melt-quenching technique, following the same procedure as in Ref. (26). The obtained glass was used as a target to coat polished c-plane sapphire substrates (thickness 430 μm) by off-axis pulsed laser deposition (PLD), following the procedure in Ref. (26). The thin film thickness was between 1-2 μm.Then, the uncoated silica glass substrate (500 μm thickness) was then placed over the BTS.2SiO_2-coated sapphire substrate leaving the BTS.2SiO_2 thin film in between. A custom-made arrangement fixture was used in order to bring both substrates in close proximity.

A pulsed 5nanosecond Nd: YAG laser (Xiton Photonics Laser) implemented into a microSTRUCT C laser micromachining workstation (3D-Micromac AG) was employed. A galvanometer scanner unit was used, in which the laser beam moves over the workpiece that remains fixed. The wavelength used was 532 nm. An objective of 255 mm focal length was employed and the beam diameter is 23 μm. In the LTB approach, the laser beam goes through the silica glass substrate and is precisely focused at the BTS.2SiO_2 interface. The focus position was corrected taking into account the shift of focal length when passing across a material.[26,29] A *wobble* beam trajectory was used.[6,24,30] Optimized laser parameters of both, BTS.2SiO_2 and BTS.3SiO_2 glass sealant systems are displayed in Table 2.

A pattern of parallel lines forming a 5 × 5 cm^2 square was irradiated over the package. Each line was irradiated several times (passes) in a bidirectional mode, to favor the heat accumulation. The distance between irradiated lines was optimized to 100 μm to ensure an approximate 50% overlap of the lines and thus, a fully bonded area, based on our previous works.[26]

The bond quality was evaluated by scanning acoustic microscopy (SAM). A SAM400 (PVA TePla Analytical Systems GmbH) acoustic microscope was employed in combination with an ultrasonic transducer (Siegert TFT) with 175 MHz center frequency and a focal length of 4 mm in water. For acoustic coupling, the samples were submerged in de-ionized and degassed water at 21°C. The employed set-up and analysis parameters are similar to our previous works.[24–28]

TABLE 2 Laser parameters employed for the laser welding of fused silica/sapphire

Silica/BTS.xSiO_2/Sapphire	Frequency (kHz)	Fluence (J/cm^2)	Scan speed (mm/s)	Passes
X = 2	35	8.53	5	20
X = 3	35	11.55	2, 5	20

Bonded samples were examined with an optical microscope (Leica DM RXE-650H). Fluorescence maps were recorded in the same optical microscope by locating an UV Lamp Camag (254 nm excitation wavelength with excitation density of 1.2 mW/cm^2) in front of the package. The fluorescence was collected with 50 seconds of acquisition time using a Leica digital camera as a detector system incorporated into the microscope.

The microstructure of the bond interface was evaluated by scanning electron microscopy (SEM) and transmission electron microscopy (TEM), by preparing a cross-sectional samples, following the same procedures as in Ref. (26). A Carl Zeiss Supra 55VP SEM microscope was employed. For TEM inspection of the interface, the sample preparation in Ref. (26) was followed. Bright field images were recorded with a FEI Tecnai G2 F20 microscope operating at 200 kV.

The mechanical characterization was carried out by pull tests. The tensile stress of three selected bonded samples were determined, following the same procedure as in Ref. (24). A tensile load perpendicular to the bonded area was applied with 1 mm/s displacement rate. A Zwick/Roell 1445 tensile testing machine was employed. The load-displacement curve was recorded up to failure.

3 | RESULTS AND DISCUSSION

3.1 | Sealing glass-ceramics for SOFC—Paste technology and conventional furnace sealing

3.1.1 | Selection of suitable glass compositions for sealing

The studied glass compositions are displayed in Table 3. The starting system is BaO–MgO–SiO_2, the glass-forming region in this system was deeply studied in Ref. ([31]) together with the definition of compositions with more suitable dilatometric properties. One of the main reasons for selecting this system was the good fit of TEC of barium silicate phases with those of the cell components. The good fit in TEC is a key issue to avoid the physical separation of the seal which provoke poor gas-tightness and stack performance. In the SOFC stack design, the sealant is in direct contact with the interconnect and the electrolyte of the half-cell. As an interconnect material, two steels are mainly used nowadays, Crofer22APU and Crofer22H that possess a TEC of 11.2·10^{-6} K^{-1} between 20°C and 500°C.[31,32] The electrolyte of the half-cell (electrolyte/anode) is 8YSZ (8 mol%. yttria-stabilized-zirconia) which presents α of 10.5·10^{-6} K^{-1}[33] and is one of the materials most widely used as an electrolyte for SOFC.

A ratio BaO/MgO = 1.5 was selected within the system BaO–MgO–SiO_2, since glass-ceramics with better adjusted

TABLE 3 Sealant compositions (% mol)

Name	SiO_2	BaO	SrO	MgO	ZnO	B_2O_3	System
55(Ba)	55	27	–	18	–	0	$BaO–MgO–B_2O_3–SiO_2$
5B(Ba)	50	27	–	18	–	5	
7.5B(Ba)	47.5	27	–	18	–	7.5	
10B(Ba)	45	27	–	18	–	10	
15B(Ba)	40	27	–	18	–	15	
55(Sr)	55	–	27	18	–	0	$SrO–MgO–B_2O_3–SiO_2$
5B(Sr)	50	–	27	18	–	5	
7.5B(Sr)	47.5	–	27	18	–	7.5	
10B(Sr)	45	–	27	18	–	10	
15B(Sr)	40	–	27	18	–	15	
Zn-55(Ba)	55	27	–	10	8	0	$BaO–ZnO–MgO–B_2O_3–SiO_2$
Zn-5B(Ba)	50	27	–	10	8	5	
Zn-7.5B(Ba)	47.5	27	–	10	8	7.5	
Zn-10B(Ba)	45	27	–	10	8	10	
Zn-15B(Ba)	40	27	–	10	8	15	
Zn-55(Sr)	55	–	27	10	8	0	$SrO–ZnO–MgO–B_2O_3–SiO_2$
Zn-5B(Sr)	50	–	27	10	8	5	
Zn-7.5B(Sr)	47.5	–	27	10	8	7.5	
Zn-10B(Sr)	45	–	27	10	8	10	
Zn-15B(Sr)	40	–	27	10	8	15	

properties could be obtained.[34] The starting composition is $55SiO_2–27BaO–18MgO$ (% mol.) (55(Ba)). This composition presented the best dilatometric properties and a suitable sintering-crystallization behaviour required for these materials.[34] Different modifications have been done to this composition to better adjust the adherence and chemical properties.

Boron oxide (B_2O_3) additions have been carried out to improve the adherence of the glass sealants to the interconnect substrate, and SiO_2 was partially substituted by B_2O_3 providing the quaternary system $BaO–MgO–B_2O_3–SiO_2$. B_2O_3 is very often used in the design of glass sealants. This compound generally provokes a reduction of T_g, T_d, viscosity, and glass stability but it improves the flow and wettability on the substrate and so, the adherence.[2,35–37] Other effect will be the delay of crystallization and chromates formation. The percentage of substitution of SiO_2 for B_2O_3 must be minimized since this oxide is less stable than the alkaline earth oxides and has tendency to volatilize at the operation temperatures of the stack due to its low melting point and high vapor pressure.[38] B_2O_3 can form volatile compounds with water vapor that can lead to seal degradation. For example, in glasses without alkali, it reacts with water-forming HBO_2 gas and breaking the glass network.[39] Other problem derived from the use of this oxide is the corrosion in reductant wet atmosphere (H_2/H_2O), obtaining gas products such as $B_3H_3O_6$ which induce the weight loss of the seal and so its degradation.[38,40,41]

BaO has been also totally substituted by SrO in order to study the quaternary system $SrO–MgO–B_2O_3–SiO_2$. This substitution has been carried out with the objective of avoiding the barium chromate formation of very high thermal expansion coefficient that provokes the physical separation and delamination of the seal. The strontium oxide can also lead to the formation of $SrCrO_4$ in oxidant conditions; this oxide also possesses a high TEC. Nevertheless, the formation of $SrCrO_4$ takes place in less extend than $BaCrO_4$, due to the higher free Gibbs energy of $BaCrO_4$ (-207 kJ/mol) than that of $SrCrO_4$ (-144 kJ/mol), calculated under the same conditions.[42,43]In both cases is negative but favorable toward the chromate formation. SrO also provokes modifications in the glass properties such as CTE, T_g, and T_d,[35] and act in a certain system as an nucleating agent stimulating crystallization.[36,37]

In the two systems in which B_2O_3 is added, a partial substitution of MgO for ZnO has been carried out providing the systems $BaO–ZnO–MgO–B_2O_3–SiO_2$ and $SrO–ZnO–MgO–B_2O_3–SiO_2$. ZnO was employed as a reductant agent and to improve the glass flow properties[35,37] to improve its wettability and adherence on the substrate. The addition of this oxide improves the sintering and crystallization

processes and slightly diminishes the value of T_g, T_d, and CTE.[44] The addition of ZnO also delays the chromates formation.[45]

The compositions with the explained modifications are presented in Table 3.

3.1.2 | Dilatometric properties

All the compositions have been characterized according to the dilatometric properties (α or TEC), T_g, and T_d; the TEC was calculated between 200°C and 500°C in order to compare the values for all compositions (Table 4).

The dilatometric curves for this system are represented in Figure 1. It is possible to observe the effect of the different substitutions on the TEC, T_g, and T_d in each system. The system with $BaO–B_2O_3$ presents TEC between 9.3 and $9.8{\cdot}10^{-6}$ K^{-1} and the same with ZnO between 9.1 and $9.5{\cdot}10^{-6}$ K^{-1}. Moreover, the systems with $SrO–B_2O_3$ and $SrO–B_2O_3–ZnO$ show α between 8.6 and 9.2 and between 8.5 and $8.9{\cdot}10^{-6}$ K^{-1}, respectively. The α value depends on the glass network stability. The incorporation of oxide modifiers creates network discontinuity points leading to a diminution of the network cohesion and provoking that the glass network stability is affected by the temperature. The cohesion of the glass network is influenced by the intensity of the bonds between oxygen and cation modifiers, this intensity is directly related to the field intensities of the cations. When the field intensity diminishes, it diminishes the intensity of the bonds between oxygen and cations leading to a less stability of the glass network and the glass presents a higher TEC. The field intensity decreases according to: Zn^{+2}> Mg^{+2}> Ca^{+2}> Sr^{+2}> Ba^{+2}.[46]

The addition of B_2O_3 does not affect the TEC value, this property remains practically constant when increasing the amount of this oxide, and this relationship is fulfilled for all the studied systems. Considering the low α of B_2O_3[46,47] and according to some authors,[36] the incorporation of this oxide in the glass composition should provoke a decrease of TEC but this was not experimentally observed in the concentration range 0-15 B_2O_3 mol%.

By the contrary, the boron addition affects T_g and T_d, as observed in Table 4 and Figure 2. When increasing the boron mol%, it takes place a diminution of T_g and T_d. The same behavior is observed for all systems. The diminution of T_g and T_d is attributed to the fact that boron oxide is a low-temperature glass former which provokes the decrease of viscosity and a weakening of the glass network [36]. This weakening is also explained due to the greater presence of tri-coordinated boron [BO_3] with planar structure than boron tetrahedral units [BO_4].

When comparing the systems with BaO and SrO (without ZnO), the total substitution of BaO for SrO provokes a slight diminution of α value, that diminishes between 0.3 and $0.9{\cdot}10^{-6}$ K^{-1}, this diminution is explained due to that SrO possess a TEC lower than BaO and the greater field intensity of the cation Sr^{+2} compared to Ba^{+2}.[46] This diminution causes an increase in the characteristic temperatures T_g and T_d, leading to an increase between 9°C and 29°C in T_g and between 7°C and 33°C in T_d, and TEC decreases since the glass network is more stable.

The partial substitution of MgO for ZnO does not cause significant changes in the α value in both systems with BaO and with SrO, since these two compounds have similar TEC and field intensity.[46,47] By the contrary, this substitution has an effect on T_g and T_d causing a diminution of these temperatures when adding ZnO in both systems. These diminutions are in a range between 2°C and 15°C in T_g and 2 and 18°C in T_d for the system with BaO. For the system with SrO, the diminution in the temperatures seems more pronounced, between 16°C and 25°C for the T_g and between 20°C and 27°C for T_d. These diminutions can be due to a decrease in viscosity when adding ZnO.[37] The values of the glasses with ZnO suggest a weakening of the glass network and a diminution of viscosity since this oxide does not only act as a modifier oxide (forming nonbridging oxygens) but it also acts as a former oxide in the silica network from an addition of 8 mol%.[44]

Considering the CTE of the materials to be sealed, suitable glass sealants must have a CTE between 9 and $12{\cdot}10^{-6}$ K^{-1}. All compositions with values outside this range

TABLE 4 Dilatometric properties of the glasses

Composition	$\alpha_{200°C\text{-}500°C}$ $\cdot10^{-6}$ K^{-1} ± 0.5	T_g (°C) ± 2	T_d (°C) ± 5
55(Ba)	9.3	718	753
5B(Ba)	9.5	669	707
7.5B(Ba)	9.7	655	700
10B(Ba)	9.6	648	690
15B(Ba)	9.8	634	671
Zn-55(Ba)	9.5	708	751
Zn-5B(Ba)	9.5	654	695
Zn-7.5B(Ba)	9.1	653	683
Zn-10B(Ba)	9.1	640	672
Zn-15B(Ba)	9.4	630	658
55(Sr)	8.6	727	760
5B(Sr)	8.9	694	740
7.5B(Sr)	8.8	683	714
10B(Sr)	9.2	675	714
15B(Sr)	9.2	663	697
Zn-55(Sr)	8.5	703	733
Zn-5B(Sr)	8.7	669	714
Zn-7.5B(Sr)	8.8	662	688
Zn-10B(Sr)	8.6	657	687
Zn-15B(Sr)	8.9	647	677

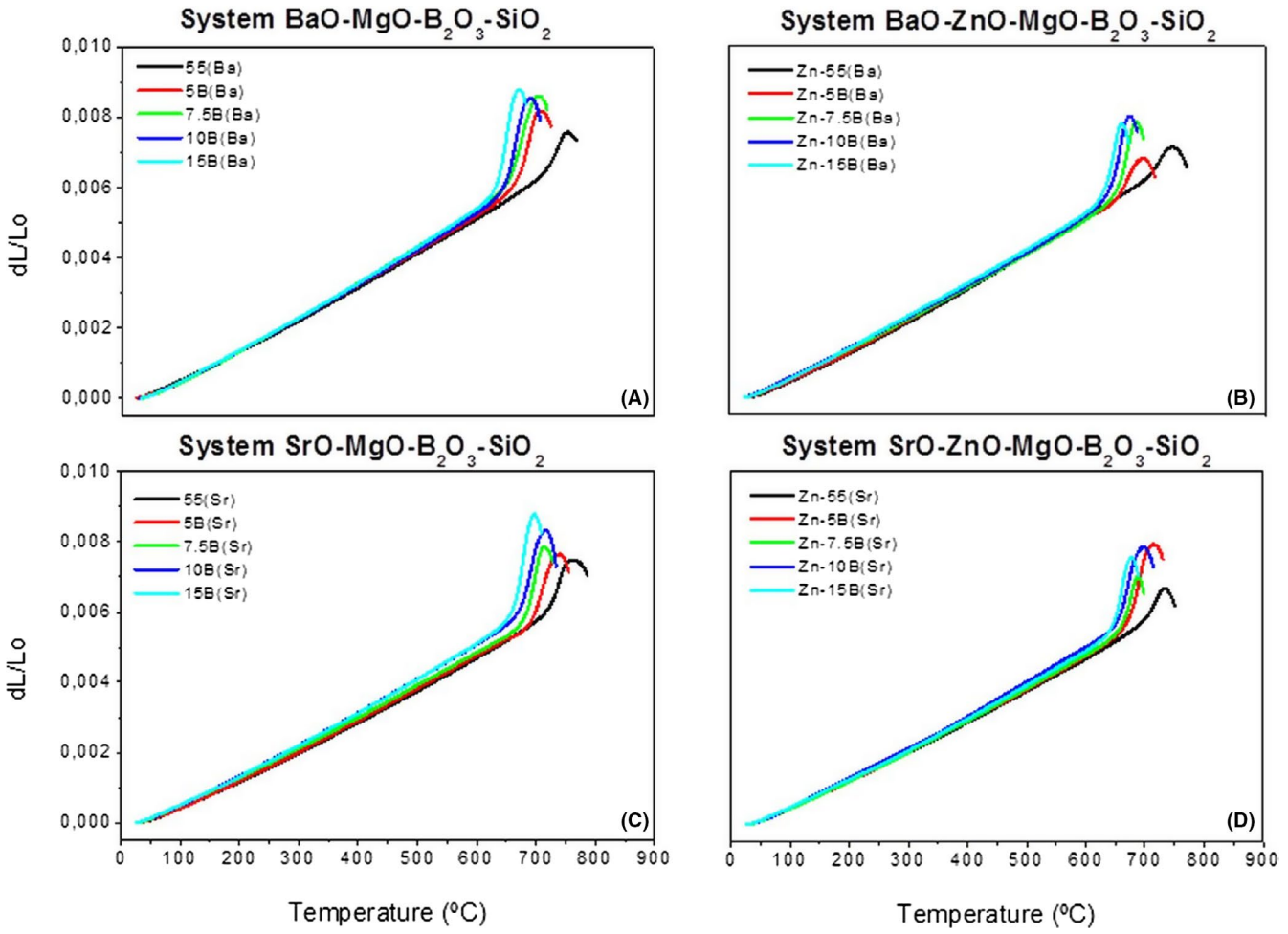

FIGURE 1 Dilatometric properties of the glasses in the systems (A) BaO-MgO-B_2O_3-SiO_2, (B) BaO-ZnO-MgO-B_2O_3-SiO_2, (C) SrO-MgO-B_2O_3-SiO_2, and (D) SrO-ZnO-MgO-B_2O_3-SiO_2

have, therefore, been discarded, including glass compositions in the system SrO–ZnO–MgO–B_2O_3–SiO_2 which show a CTE between 8.5 and $8.9 \cdot 10^{-6}$ K^{-1} and compositions 55(Sr), 5B(Sr), and 7.5B(Sr) of the system SrO–MgO–B_2O_3–SiO_2 which present values of CTE of 8.6, 8.9, and $8.8 \cdot 10^{-6}$ K^{-1}, respectively.

3.1.3 | Sintering and adherence of the glasses

Due to the importance of obtaining well-densified glass-ceramics and with low porosity, HSM has been employed for the study of the sintering behavior and also as a first approximation to know the possible adherence of the original glass sealants.

In order to identify the compositions that present a good adherence with the interconnect material; the HSM has been carried out on Crofer22APU as a substrate. The heating rate for the SOFC is slow and around 2°C/min, in order to avoid the differences of temperature that provoke stresses and possible curvatures or cracks in the materials that form the cell; for this reason, the same heating rate was employed simulating the heating conditions of the cell and only up to 1000°C to prevent the possible softening of the steel substrate. The same particle size was used for all the compositions ($\varphi < 63$ μm) with the objective to avoid the effects of the particle size on sintering and be able to compare the compositions. The cylindrical samples were manually pressed to obtain similar initial packing degree. The obtained curves for all the studied systems are represented in Figure 2 in which A is the area of the sample shade at each temperature observed in the HSM and A_0 is the initial area of the sample shade.

The sintering process occurs at temperatures slightly higher than T_g after the activation of viscous flow.[48] The studied system presents a diminution in the area between 60% and 70% that correspond with a contraction between 40% and 30%. The partial substitutions of SiO_2 for B_2O_3 provoke in all systems an acceleration of the sintering process that starts at lower temperatures. The substitutions also affect the rest of characteristic temperatures.

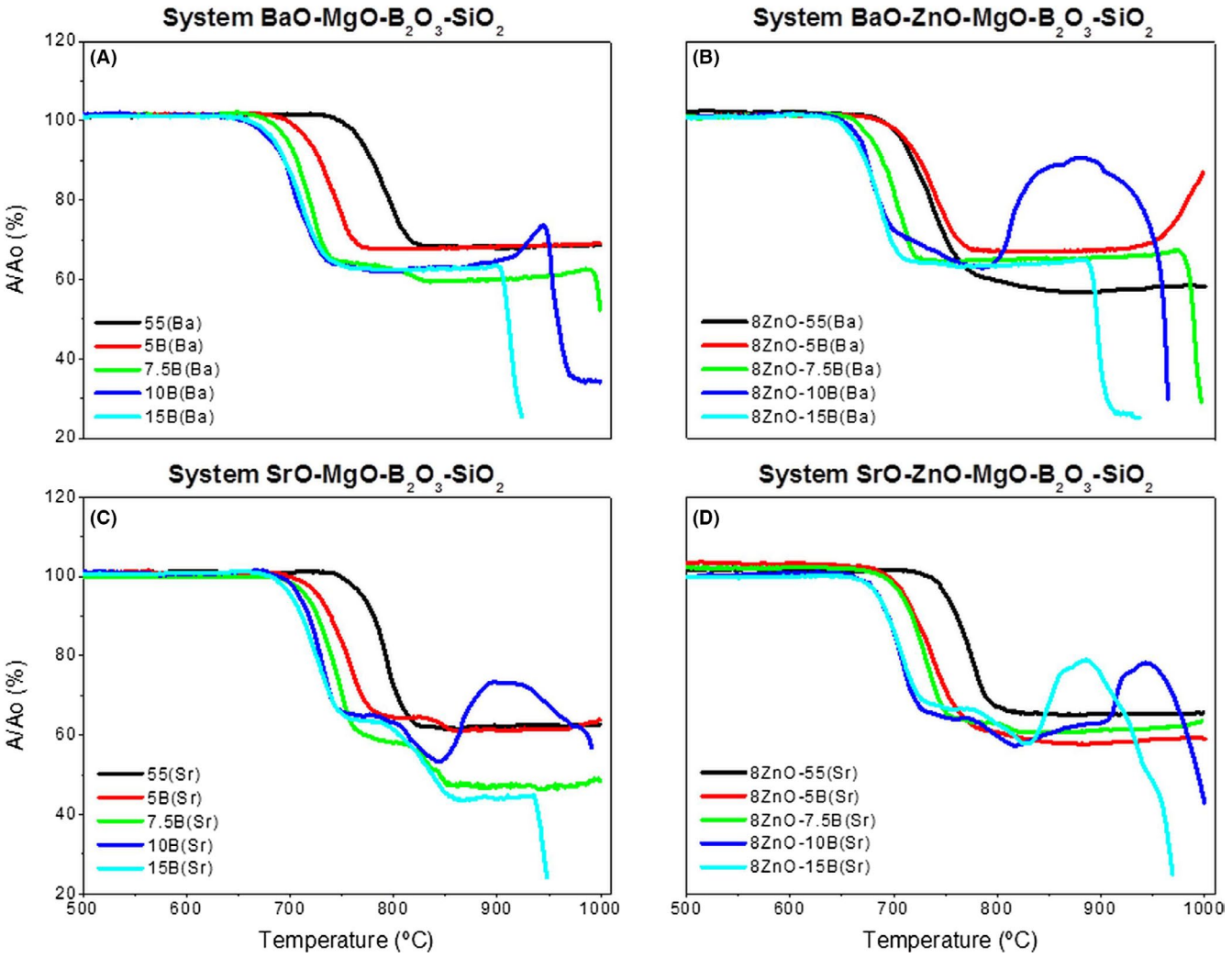

FIGURE 2 Variation of the area/area$_0$ as a function of temperature measured by hot-stage microscopy of the glasses within the systems: (A) BaO-MgO-B_2O_3 -SiO_2, (B) BaO-ZnO-MgO-B_2O_3 -SiO_2, (C) SrO-MgO-B_2O_3 -SiO_2, and (D) SrO-ZnO-MgO-B_2O_3 -SiO_2 in powder ($\varphi < 63$ μm) and at 2°C/min up to 1000°C on a Crofer22APU substrate

The systems containing ZnO (Figure 2B,D) also present the same behavior; the partial substitution of MgO for ZnO provokes an acceleration of the sintering process as with B_2O_3. This is explained due to that these two oxides (B_2O_3 and ZnO) modify the viscosity increasing fluency and wettability on the substrates.[2,35–37] When comparing the systems with BaO and SrO (Figure 2A,C), the total substitution of BaO for SrO leads to a delay of the sintering process, so the compositions within the system with SrO sinter at higher temperatures.

Some compositions present an expansion in the area at high temperatures, this expansion take place after the maximum sintering of the sample. The increase in area is associated with a foaming phenomenon and degasification that increase with the particle size diminution.[49] The main source of foaming effect is the CO_2 absorption in the powder surface during trituration, milling and storage, and processing of the glasses.

The characteristic temperatures determined from the sintering curves and the images of HSM are represented in Table 5.

Table 5 shows the temperatures associated with the processes of beginning of sintering, maximum sintering, softening, half-ball, and fluency. The last column indicates if there was joining with the steel after the experiment. The compositions with higher silica content and more refractory ones do not reach the softening, half-ball, and flow temperatures, presenting a wide separation between sintering and the rest of processes. The compositions that do not soften (T_S) before 1000°C do not present union with the substrate as it can be observed in the last column of Table 5.

The glass compositions that do not reach the half-ball (T_{HB}) before 1000°C present poor bonding with the substrate since the glass must soften and flow sufficiently in order to allow wetting and adherence between the seal and the substrate. By the contrary, the compositions reaching the T_{HB} present a good union with the steel.

Important properties for a proper selection of glass compositions are the sintering and adhesion of the sealants.

TABLE 5 Characteristic temperatures obtained by hot-stage microscopy

Composition	T_{FS} (°C)	T_{MS} (°C)	T_S (°C)	T_{HB} (°C)	T_F (°C)	Union with Crofer22APU
55(Ba)	757	808	/	/	/	No
5B(Ba)	706	763	/	/	/	No
7.5B(Ba)	695	736	796	998	/	Yes
10B(Ba)	683	730	771	954	966	Yes
15B(Ba)	675	727	757	910	925	Yes
Zn-55(Ba)	702	766	/	/	/	No
Zn-5B(Ba)	699	763	932	/	/	Yes
Zn-7.5B(Ba)	680	720	980	987	991	Yes
Zn-10B(Ba)	660	694	753	957	962	Yes
Zn-15B(Ba)	653	701	747	895	938	Yes
55(Sr)	771	815	992	/	/	Yes
5B(Sr)	719	776	818	/	/	Yes
7.5B(Sr)	712	760	791	852	/	Yes
10B(Sr)	709	742	784	839	997	Yes
15B(Sr)	694	745	770	835	949	Yes
Zn-55(Sr)	740	788	847	/	/	Yes
Zn-5B(Sr)	712	757	797	/	/	Yes
Zn-7.5B(Sr)	696	748	790	/	/	Yes
Zn-10B(Sr)	682	722	773	974	989	Yes
Zn-15B(Sr)	678	723	755	831	970	Yes

Abbreviations: T_{FS}, temperature of beginning sintering; T_{MS}, temperature of maximum sintering; T_S, softening temperature; T_{HB}, half-ball temperature; T_F, flow temperature.

Considering the HSM results, compositions which do not reach T_S before 1000°C do not bond properly with the substrate. Such compositions were, therefore, discarded as seals for SOFC with planar configuration that use Crofer22APU or Crofer22H steel as an interconnect since they may soften if they exceed this temperature. The limitation of the sealing temperature helps to minimize the diffusion of elements from steel into the seal. Thus, the potential negative impacts of such diffusion on crystallization of the seal and steel corrosion can also be limited.

Glasses which do not reach T_{HB} before 1000°C were also discarded as these compositions do not soften enough to wet the substrate properly and obtain a gas-tight joint with the steel, one of the key requirements of these materials. Compositions with high silica contents of 55 and 50 mol % are discarded for this reason.

ZnO-containing compositions have also been discarded for this application as ZnO increases the conductivity of seals leading to noncompliance of resistivity requirements. The ZnO addition also brings about an increase of steel corrosion in a dual atmosphere.[50]

The remaining compositions were selected with the aim of trying to decrease the B_2O_3 content to the minimum amount due to the volatility problems it may present. With this aim, it was decided to maintain the concentration of this oxide not higher than 10% mol.

In view of the entire discussed factors, two suitable compositions were selected. Compositions 7.5B(Ba) and 10B(Sr) were selected since both exhibited a suitable TEC, sintering behavior and good adhesion to the substrate.

3.2 | Joints of steel/glass-ceramic/half-cell

In the cell design, the glass-ceramic sealant is in direct contact with the electrolyte of the half-cell, so it is very relevant to study the joints between the glass-ceramics and this material to evaluate the quality and response vs thermal cycling. Half-cells are formed by a dense electrolyte of ~ 15 μm thickness of 8YSZ and a porous anode constituted by a cermet Ni-8YSZ. Unions with the half-cell and the steels Crofer22APU and Crofer22H were prepared with the two selected compositions.

Figure 3 shows the results obtained for composition 7.5B(Ba) and Figure 5 for composition 10B(Sr) both after sealing at 850ºC for 10 hours. Both joints present a good adherence with electrolyte and steel.

In the case of barium composition, a great degree of crystallization at the interphase is observed with the apparition of

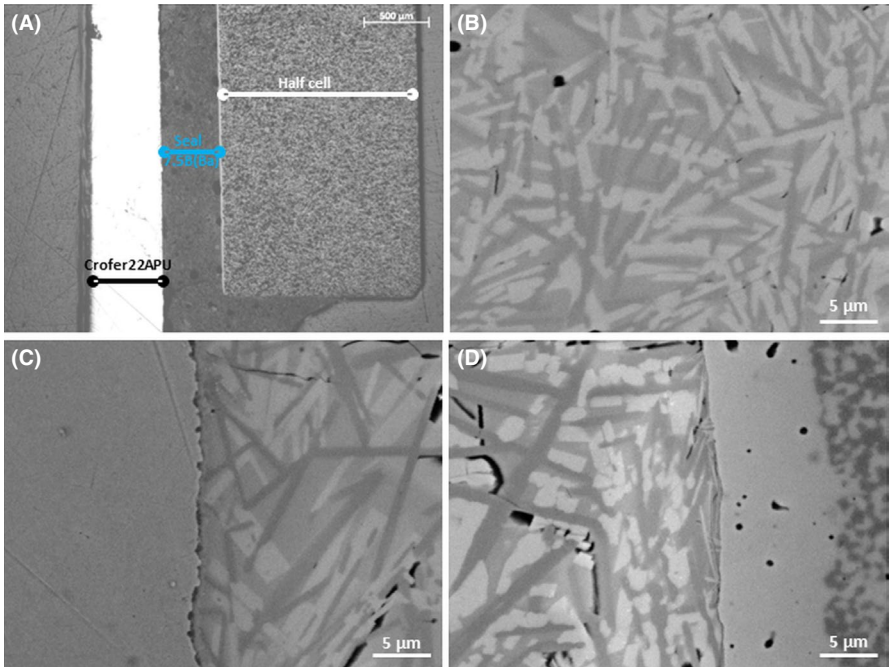

FIGURE 3 Union Crofer22APU-glass-ceramic-8YSZ of composition 7.5B(Ba) sealed at 850°C during 10 h. (A) General view. (B) Glass-ceramic microstructure. (C) Interphase steel-sealant. (D) Interface sealant-8YSZ

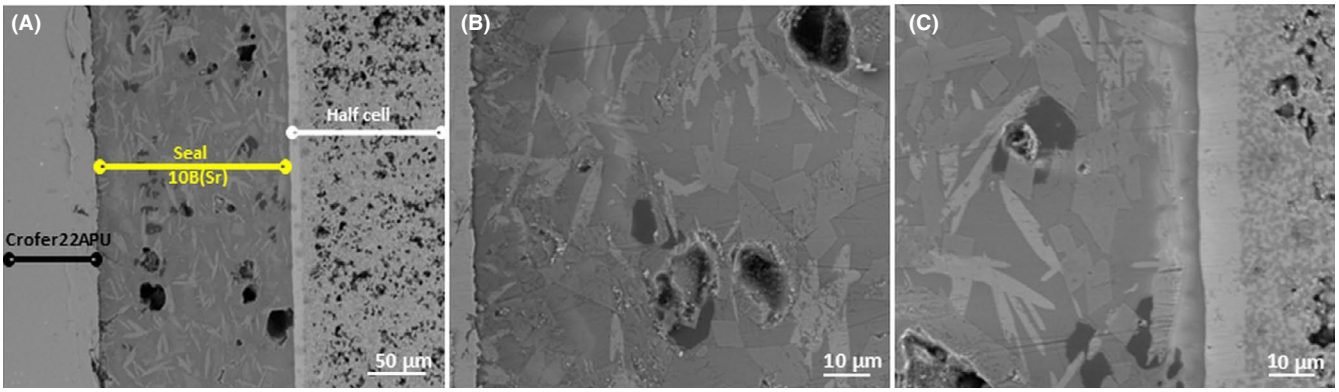

FIGURE 4 Union Crofer22APU-glass-ceramic-8YSZ of composition 10B(Sr) sealed at 850°C for 10 h. (A) General view. (B) Interphase steel-sealant. (C) Interphase sealant-8YSZ

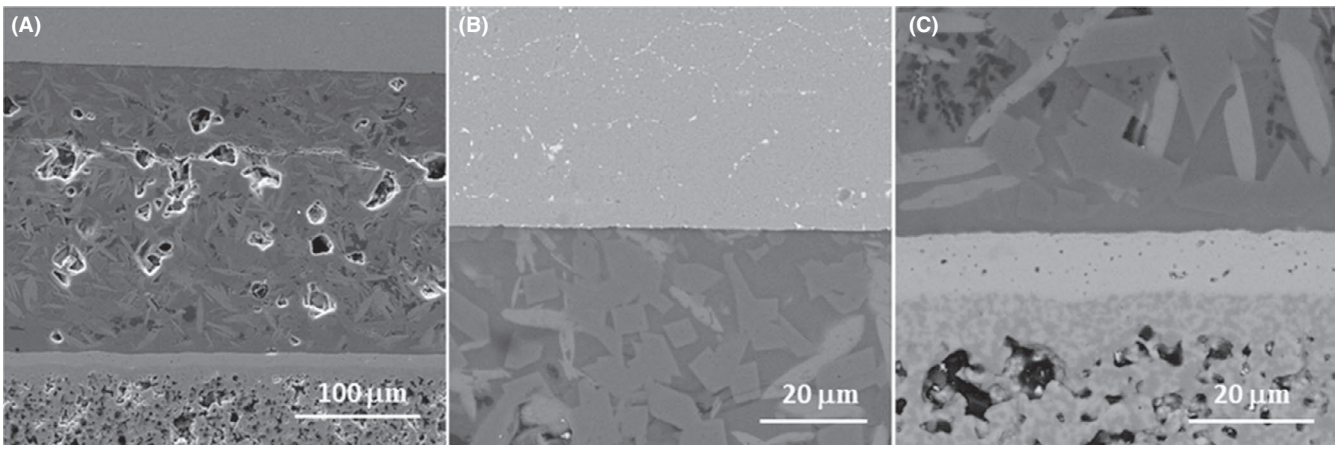

FIGURE 5 Union of Crofer22H-glass-ceramic-8YSZ of composition 10B(Sr) sealed at 850°C for 10 h and thermally cycled (50 cycles). (A) General view. (B) Interphase steel-sealant. (C) Interphase sealant-8YSZ

some small cracks (superior zone Figure 3D) probably due to differences between TEC between these two materials.[51] No delamination is observed at the interface but only small cracks are discerned.

The strontium composition shows a clean and continuous interface with the electrolyte without the presence of crack or voids (Figure 4). There is no reaction zone or formation of any intermediate layer. In general, the joint seal 10B(Sr)/electrolyte shows bigger stability than that of composition 7.5B(Ba), probably due to the higher stability of TEC of this glass-ceramic that keeps approximately constant with the crystallization time.[51] This composition seems to show better chemical compatibility with the electrolyte.

The glass-ceramic of composition 10B(Sr) was selected for a thermal cycling study (50 cycles) since its union with the electrolyte (8YSZ) present the best characteristics. After thermal cycling, the sample cross-section was studied (Figure 5).

The interfaces after thermal cycling show an excellent union which demonstrate a good resistance vs thermal shock of the glass-ceramic and the joints with the electrolyte and the steel Crofer22H. Both interphases are clean and continuous without cracks or voids, indicating a good chemical compatibility at the interphase. Figure 6 shows the elemental mapping by EDX of the interphase seal/electrolyte in which no significant interfusion of the electrolyte elements into the glass-ceramic and vice-versa is observed. The dissolution of 8YSZ grains is not observed, neither the formation of compounds such as $SrZrO_3$ at the interphase, differently to other glass sealants containing SrO[52] based in the glass system Ga_2O_3–SiO_2–B_2O_3–Na_2O–K_2O–CaO–SrO.

The phase $Sr_2MgSi_2O_7$, a SiO_2-rich phase, and the phase $SrMgSi_2O_6$ can be recognized by means of the elemental mapping. The crystallizing phases were well-described in a previous paper.[53]

Mechanical strength of these joint systems is reported in Refs. (51) and (53).

3.3 | Laser welding of fused silica and sapphire through a BTS $xSiO_2$ (x = 2, 3) glass thin film as sealant

This section represents a particular case of laser transmission bonding (LTB). Optical transmission of silica is above 90% over a broad range of the spectrum. Thus, the laser beam goes through it and efficiently deposits thermal energy in the BTS. $xSiO_2$ (x = 2, 3) interface (Figure 7A). In comparison with previous works on BTS-glass thin film sealant,[24,25] the enrichment in SiO_2 was performed to better fit the CTE requirements. The difference in CTEs of silica glass and sapphire

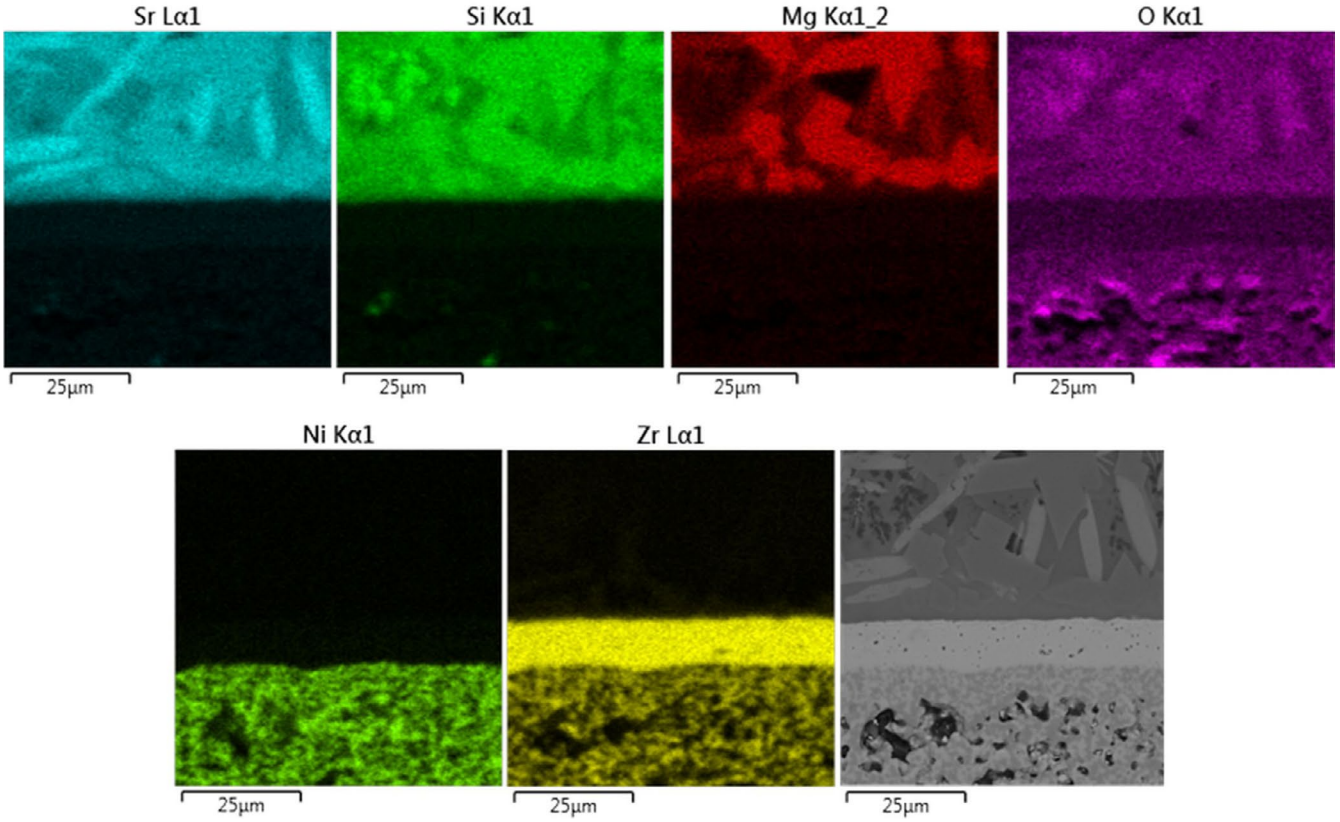

FIGURE 6 Elemental mapping by EDX of the joint sealant-8YSZ, glass-ceramic 10B(Sr) sealed at 850°C during 10 h and thermally cycled (50 cycles)

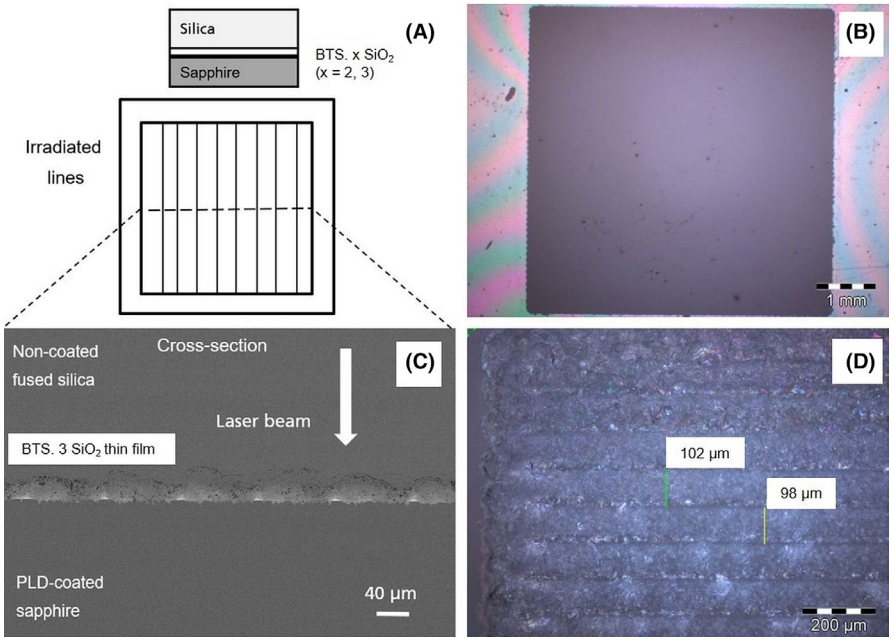

FIGURE 7 (A) Sketches of the employed setup for the *sandwich* configuration and the irradiated pattern of parallel lines forming a square; (B) Overview top-view micrograph of the joined fused silica substrate and the sapphire substrate through the BTS.2SiO_2 thin film by focusing on the upper silica glass; (C) SEM micrograph of the cross-section of the joined sample through the BTS.3SiO_2 thin film. The direction of the laser beam by entering the sample is marked; (D) Top-view micrograph of the joined bond interface showing the irradiated lines (silica substrate up)

is one order of magnitude, being $0.55.10^{-6}$ and 6.10^{-6} K^{-1}, respectively. CTE of BTS glass is $9.8.10^{-6}$ K^{-1}. However, by increasing the SiO_2 content, the CTE decreases, until 7.9 10^{-6} K^{-1} for the BTS.2SiO_2 glass, making it more compatible to the CTE of the joined substrates. Nonstoichiometric BTS glasses, with molar composition BTS.xSiO_2, (x = 0-3) has been reported.[54] For x = 2.5, BTS forms a eutectic with SiO_2.

Following our previous work in Ref. (26) employing a BTS.3SiO_2 thin film, the laser welding of both substrates was successfully achieved by employing the BTS.2SiO_2 glass thin film as a sealant. After the laser process, both substrates remain welded. The surface of the upper silica substrate was not damaged under the laser beam, indicating a very efficient focus in the intermediate layer. Figure 7B shows a top view micrograph of the bonded sample, in which the irradiated square pattern composed of parallel lines is observed with the naked eye, in contrast with the transparency of the nonirradiated area. Interference rings are observed in the nonirradiated (nonbonded) area (Figure 7B). The appearance of Newton rings exclusively in the nonirradiated area is a first indication of the successful joint. The origin of these rings is the interferences of light due to the gap in the nanometer range between both substrates in the nonbonded area.

By focusing in the interface, a coarse-grained microstructure is observed (Figure 7D), in which the irradiated lines are discerned. The line broadness increases by employing the wobble trajectory of the beam, (around 100 µm in Figure 7D), in comparison with a straight beam trajectory.[24] Figure 7C displays a new cross-section SEM image of the bonded sample reported in[26] employing the BTS.3SiO_2 thin film. The bond interface is clearly observed, in which both substrates are joined. Each bump observed in Figure 7C corresponds to the cross section of one of the irradiated lines. The pristine thin film is observed between the bumps (Figure 7C), in those regions not reached by the laser beam. The upper silica substrate presents some microfractures in the interface with the BTS bumps. In the interior of the thin film, some inhomogeneities are discerned. In nanosecond laser regime, the interaction of the laser beam with the bond interface is characterized by the formation of a plasma plume in this region. This plasma expands in direction of the laser beam, perpendicular to the surface of the sample.[55] Due to the sandwich configuration, the plasma plume is stopped by the upper silica substrate, leading its partial ablation in the bond interface, as shown in Figure 7C. The BTS.xSiO_2 thin film is completely molten (Figure 7C), welding both substrates when resolidified. From our previous works,[6,24–26] it is well-known that the ablation of the upper substrate upon laser irradiation leads to its partial incorporation (in this case silica) in the thin film. Hence, the composition of the glass sealant changes with the course of the laser welding, incorporating constituents of the upper wafer. This is especially important in the case that several passes are used (Table 2), since the glass sealant is slightly changing its absorption properties after each individual pass. Thus, the heat accumulation induced by the laser interaction must be high enough to overcome any decrease of optical absorption. Not only several passes, but also lower scan speeds and high repetition rates are preferred in laser welding processes to favor the heat accumulation.

In the particular case of BTS-based glasses, the photodarkening effect must be considered. Photodarkening is produced from the reduction of polyvalent elements, like titanium in BTS, upon irradiation with nanosecond lasers. The optical

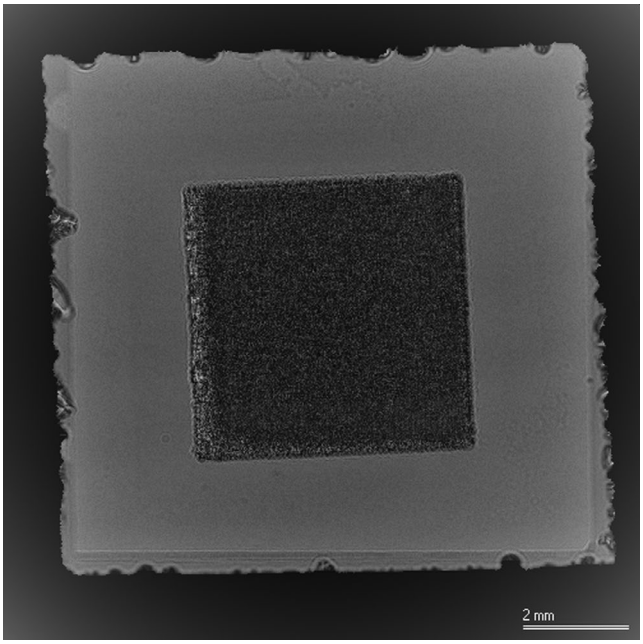

FIGURE 8 SAM micrograph of the joined fused silica substrate and the sapphire substrate through the BTS.2SiO_2 thin film

absorption increases toward the end of each individual pulse. This effect contributes also to the ablation of the upper silica substrate, due to the high thermal energy produced.

In order to evaluate the bonded area, the sample was subjected to SAM inspection (Figure 8). SAM is a nondestructive technique used to characterize bonded interphases, among others. It is possible to discern structural defects of the bond interface, as a function of the depth with a resolution in the μm range. SAM micrographs are digitalized in the way that nonbonded areas, in which the water used as medium in the SAM measurements is located between both substrates, is displayed in light gray color. Bonded areas, (without gaps between both substrates), are shown in a darker color. The irradiated squared pattern appears darker than the surrounding nonirradiated area (Figure 8), indicating a general good bond quality. However, some heterogeneities can be discerned, indicating not fully welded points. This is good agreement with the heterogeneities observed in the bond interface (Figure 7C). The bonded area was quantified through image analysis, giving 20 mm^2 of bonded area from the irradiated 25 mm^2 (5 × 5 mm^2 square), which corresponds to 80% of bonded area in the irradiated pattern.

The bonded sample was then exposed to UV light, in order to qualitatively evaluate the BTS crystallization from its characteristic blue emission. A white-bluish emission is visible by naked eye over the whole irradiated area, as shown in Figure 9, which would indicate BTS crystallization. It is important to note, that the pristine BTS–2SiO_2 thin film (nonirradiated area) does not show any luminescence, confirming the BTS crystallization all over the square pattern.

For the microstructural inspection of the bonded area, the BTS.3SiO_2 sample was selected.[26] Figure 10 displays the microstructure of the bond interface. Particles or round morphology below 50 nm in diameter are observed in the glass sealant in contact with the silica substrate. The presence of these particles in the bond interface supports the BTS crystallization. Surprisingly, these particles were not found in the interface with the sapphire substrate.[26] A much lower thermal conductivity of silica in comparison with sapphire would lead to a heat accumulation in the silica side, rather than in the sapphire, which acts more like a heat spreader. This heat accumulation contributes

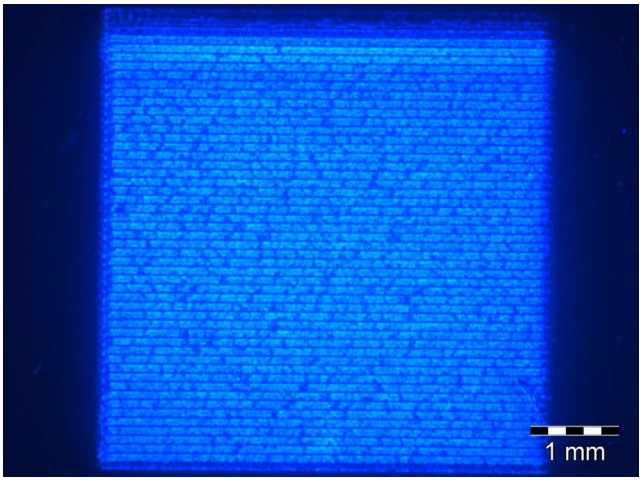

FIGURE 9 Top-view micrograph of the bonded sample through the BTS.2SiO_2 thin film under 254 nm excitation (silica substrate up)

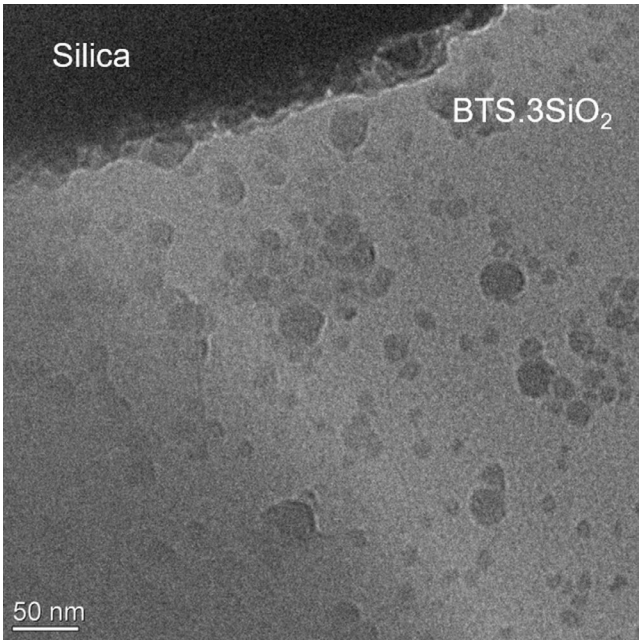

FIGURE 10 TEM micrograph of the bonded interface at the border with the silica glass substrate by employing the BTS.3SiO_2 glass thin film reported in Ref. (26)

to the structural damage observed in this interface (Figure 7C), as well. Another aspect is that Ti^{4+} is a network former (NF) in fourfold coordination. With increasing concentration of SiO_2 (from the ablation of the silica substrate), the role of Ti^{4+} as NF will be displaced to Ti^{4+} in five- and sixfold coordination, acting as a network modifier. This would favor the crystallization of BTS in the silica side, as well. Additionally, any Al incorporation from the sapphire substrate to the BTS sealant would hinder the BTS crystallization, as reported.[25] This fact highlights that not only the physical properties of the glass sealant must be taken into consideration, but also those from the substrates to be welded, especially when ablation of those occurs upon laser interaction.

In order to achieve a preliminary overview of the mechanical resistance of the bonded samples, two tests were performed:

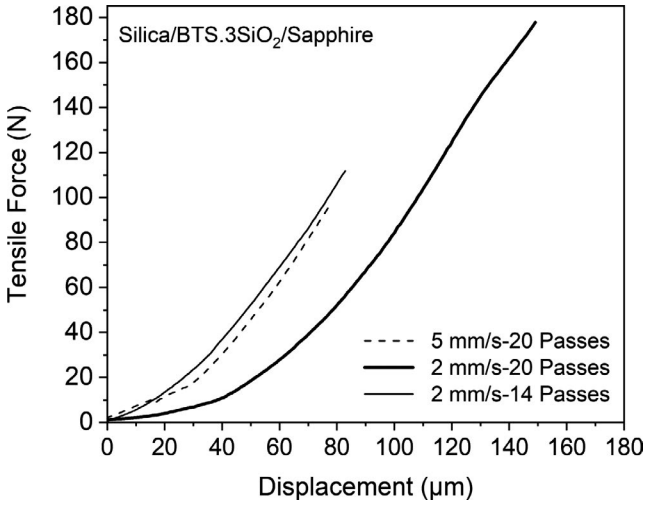

FIGURE 11 Tensile force-displacement curves for three selected laser welded sample with $BTS.3SiO_2$ as a glass sealant thin film at three different sets of laser parameters

1. Influence of the different CTE (silica, BTS, and sapphire) of the joined materials: Here the bonded sample through the $BTS.2SiO_2$ thin film was heat treated at 100°C for 30 minutes. This temperature was chosen as reference from the range of working temperatures in microfluidics, which is below 100°C depending on the system.[56] Despite this large CTE difference and the large bonded area (20 mm^2, SAM), the joined sample is stable and both substrates remain joined after the treatment. The incorporation of silica into the glass sealant upon laser welding process contributes to decrease the CTE difference.
2. Tensile tests were performed in three selected joint samples through the $BTS.3SiO_2$ glass sealant composition. The influence of the scan speed and the number of passes (Table 2) was evaluated and the values are displayed in Figure 11. On one hand, for the same number of passes, the tensile force increases at lower scan speeds. On the other hand, keeping the scan speed constant, the tensile force increases at higher number or passes. A slow scan speed gives rise to higher pulse overlaps and thus more heat accumulation. A higher number of passes also favors the heat accumulation in the glass sealant. Considering an average bonded area of 20 mm^2 from the irradiated 25 mm^2 pattern (Figure 8), the highest tensile force value of 178 N would correspond to 9 MPa of tensile stress. As reference, this value corresponds to 19% of the tensile strength of pure fused silica (47 MPa).

Although more samples should be tested for a good statistics of both, heat treatment test and tensile measurements, these preliminary results suggest that the laser welding of sapphire and silica through $BTS.xSiO_2$ (x = 2, 3) thin films is a successful approach. The mechanical characterization and evaluation of the mechanical strength of similar joint systems is reported in Refs. (24,27,28).

TABLE 6 Comparison between conventional furnace sealing- and laser welding

Furnace sealing	Laser welding
Glass sealant applied as paste from milled bulk glass Larger bonded areas	Glass sealants can be pastes or thin films Localized bonded areas (μm range). Free-shape trajectories
Control of the processing temperature	Achieved temperature difficult to estimate
Control of crystallization possible Both joint partners can be opaque (metals, ceramics)	Control of crystallization difficult. Composition of the sealant changes during the laser process For LTB, the upper substrate must be transparent. Direct bonding set-up for opaque substrates
CTE, viscosity, grain size, thermal conductivity, sintering-crystallization effects must be considered Temperature, heating rate, and time must be optimized	CTE, optical properties, and thermal conductivity must be considered Laser parameters must be optimized
Substrate remain intact at the bond interface Longer processing times	Ablation of the upper bond interface in nanosecond regime Higher processing speed
Several samples can be joint simultaneously	Samples are processed one after the other
Lower costs	Laser facilities are usually expensive

The results on the laser welding represent the feasibility of this technique to join two dissimilar transparent materials by employing a nanosecond -pulsed laser.

The comparison of the both processing methods reported here is summarized in Table 6. In both cases, the glass sealant should present a CTE value close to the join partners. However, in the case of laser welding, this is less critical, because of the limited laser-irradiated area imposed by the beam spot. The application fields in which each of these processing tools are involved is different. While the laser welding is very beneficial in the field of microelectronics and optics, due to the miniaturization of the devices, in other application fields, like SOFC fuel cells a larger bonded area achieved by the furnace method is preferable. Employment of thin film coatings is on demanding due to the incorporation of miniaturized devices and the reduced time of operation of small volumes. Moreover, nanosecond-pulsed lasers are more affordable and stable than CW and ultrashort-pulsed lasers.

4 | CONCLUSIONS

Two different approaches for joining materials through glass sealants were presented: Conventional furnace sealing and laser welding. Not only the technological procedure is different, but also the physical nature of the glass sealants. While in the furnace approach a glass paste from the milled bulk glass is usually applied, in the particular case of laser welding exposed here a thin film (1-2 μm thickness) was employed.

Sealing glass-ceramics for SOFC have been presented as an example of conventional furnace sealing in which after the application of the glass powder using paste technology, the complete stack is heated up to the operation temperature of the stack at which gas-tightness is also reached. Glass compositions in the system BaO/SrO–MgO/ZnO–B_2O_3–SiO_2 have been designed to fulfill the stack requirements and the best sealants have been selected according to their dilatometric properties, sintering and crystallization behavior, and suitable chemical compatibility. In particular, the 10B(Sr) composition shows the better stability of the joints, with the formation of a continuous, clean interface with no cracks or gaps. After thermal cycling of the Crofer22H/10B(Sr)/8YSZ joints, the interfaces exhibit excellent adhesion, with no cracks or significant diffusion of elements between the seal and the steel or the electrolyte.

In the second approach, laser bonding of transparent substrates was successfully achieved through SiO_2-enriched BTS-thin films as a glass sealant by employment of a nanosecond-pulsed laser. BTS crystallizes in the bonded interface, giving rise to a strong blue emission upon UV excitation. SiO_2 from the fused silica substrate is incorporated into the glass sealant upon laser welding process, leading to compositional changes upon laser irradiation. Mechanical properties in terms of tensile stress and heat resistance (different CTEs) are very promising. The results represent the usefulness of the laser welding to join transparent materials through BTS-based glass thin films upon nanosecond-pulsed laser interaction.

Both methods find applications in different technological fields. The selection of one of them must be based on the physical and geometrical requirements and on the working conditions of the final joint.

ACKNOWLEDGMENTS

MJ Pascual thanks the European project FP7-JTI-CP-FCH, Working toward Mass Manufactured, Low Cost, and Robust SOFC stacks (MMLRC = SOFC), project reference: 278525 and the project CNPq/PVE 400590/2013. A. de Pablos-Martín acknowledges financial support of FhG Internal Programs under Grant No. Attract 692 280. She is deeply grateful to Prof. T. Höche from Fraunhofer Institute IMWS for the opportunity to be involved in the project and his great support, to Prof. C. Rüssel of Friedrich Schiller University Jena-Otto Schott Institute, for providing fresnoite bulk glasses, to Prof. M. Lorenz's and Prof. Grundmann's group at the Leipzig University for preparation of the fresnoite thin films by PLD, and to Sebastian Tismer and M. Mittag from Fraunhofer Institute IMWS, for the SAM measurements and for the tensile test measurements, respectively. The authors thank Prof. Alicia Durán for her continuous support and teaching.

ORCID

Araceli de Pablos-Martín https://orcid.org/0000-0002-9824-6273
Maria J. Pascual https://orcid.org/0000-0002-6833-9663

REFERENCES

1. Sinhdeo NN, Shukla RK. Solder glass processing. Glass Science and Technology. New York: 2: Academic Press Inc., 1984; p. 169–207.
2. Weil KS. The state-of-the-art in sealing technology for solid oxide fuel cells. Jom-Us. 2006;58(8):37–44.
3. Singh RN. Sealing technology for solid oxide fuel cells (SOFC). Int J Appl Ceram Tec. 2007;4(2):134–44.
4. Lessing PA. A review of sealing technologies applicable to solid oxide electrolysis cells. J Mater Sci. 2007;42(10):3465–76.
5. Poprawe R. Tailored Light 2-Laser Application Technology. Berlin Heidelberg: Springer-Verlag, 2011.
6. de Pablos-Martín A, Höche T. Laser welding of glasses using a nanosecond pulsed Nd:YAG laser. Opt Laser Eng. 2017;90:1–9.
7. Faidel D, Behrl W, Gross S, Reisgen U. Glass sealing materials and laser joining process development for fuel cell stack manufacturing. Materialwiss Werkst. 2010;41(11):914–24.
8. Rodríguez-López S, Comesaña R, del Val J, Durán A, Justo VM, Serbena FC, et al. Laser cladding of glass-ceramic sealants for SOFC. J Eur Ceram Soc. 2015;35(16):4475–84.
9. Ribeiro F, MaçAira J, Cruz R, Gabriel J, Andrade L, Mendes A. Laser assisted glass frit sealing of dye-sensitized solar cells. Sol Energy Mater Sol Cells. 2012;96(1):43–9.

10. Döhler F, Kasch S, Schmidt T, Rüssel C. Sealing of alumina using a CO_2 laser and a rapidly crystallizing glass. J Mater Process Technol. 2016;233:206–11.
11. Börner F-D, Lippmann W, Hurtado A, Schön B. Glasses for laser joining of zirconia ceramics. J Eur Ceram Soc. 2014;34(3):765–72.
12. Cho SJ, Lee KH. Laser sealing of dye-sensitized solar cell panels using V_2O_5 and TeO_2 contained glass. J Korean Ceram Soc. 2014;51(3):170–6.
13. Herrmann M, Lippmann W, Hurtado A. Y_2O_3–Al_2O_3–SiO_2-based glass-ceramic fillers for the laser-supported joining of SiC. J Eur Ceram Soc. 2014;34(8):1935–48.
14. Emami S, Martins J, Madureira R, Hernandez D, Bernardo G, Mendes J, et al. Development of hermetic glass frit encapsulation for perovskite solar cells. J Phys D: Appl Phys. 2019;52(7):074005.
15. Ivanou DK, Santos R, Maçaira J, Andrade L, Mendes A. Laser assisted glass frit sealing for production large area DSCs panels. Sol Energy. 2016;135:674–81.
16. Maçaira J, Andrade L, Mendes A. Laser sealed dye-sensitized solar cells: efficiency and long term stability. Sol Energy Mater Sol Cells. 2016;157:134–8.
17. Maçaira J, Mesquita I, Andrade L, Mendes A. Role of temperature in the recombination reaction on dye-sensitized solar cells. Phys Chem Chem Phys. 2015;17(35):22699–710.
18. Wisniewski W, Thieme K, Rüssel C. Fresnoite glass-ceramics – A review. Prog Mater Sci. 2018;98:68–107.
19. Martín LL, Haro-González P, Martín IR, Puerto D, Solís J, Cáceres JM, et al. Local devitrification of Dy^{3+} doped $Ba_2TiSi_2O_8$ glass by laser irradiation. Opt Mater. 2010;33(2):186–90.
20. Honma T, Ihara R, Benino Y, Sato R, Fujiwara T, Komatsu T. Writing of crystal line patterns in glass by laser irradiation. J Non-Cryst Solids. 2008;354(2–9):468–71.
21. Lipatiev AS, Moiseev IA, Lotarev SV, Lipateva TO, Presnyakov MY, Fedotov SS, et al. Growth of fresnoite single crystal tracks inside glass using femtosecond laser beam followed by heat treatment. Cryst Growth Des. 2018;18(11):7183–90.
22. Müller A, Lorenz M, Brachwitz K, Lenzner J, Mittwoch K, Skorupa W, et al. Fresnoite thin films grown by pulsed laser deposition: photoluminescence and laser crystallization. CrystEngComm. 2011;13(21):6377–85.
23. Cabral AA, Fokin VM, Zanotto ED, Chinaglia CR. Chinaglia CR. Nanocrystallization of fresnoite glass. I. Nucleation and growth kinetics. J Non-Cryst Solids. 2003;330(1–3):174–86.
24. de Pablos-Martin A, Benndorf G, Tismer S, Mittag M, Cismak A, Lorenz M, et al. Laser-welded fused silica substrates using a luminescent fresnoite-based sealant. Opt Laser Technol. 2016;80:176–85.
25. de Pablos-Martín A, Ebert M, Patzig C, Krause M, Dyrba M, Miclea P, et al. Laser welding of sapphire wafers using a thin-film fresnoite glass solder. Microsyst Technol. 2015;21(5):1035–45.
26. de Pablos-Martin A, Lorenz M, Grundmann M, Hoche T. Laser welding of fused silica glass with sapphire using a non-stoichiometric, fresnoitic $Ba_2TiSi_2O_8.3SiO_2$ thin film as an absorber. Opt Laser Technol. 2017;92:85–94.
27. de Pablos-Martin A, Tismer S, Benndorf G, Mittag M, Lorenz M, Grundmann M, et al. Laser soldering of sapphire substrates using a BaTiAl6O12 thin-film glass sealant. Opt Laser Technol. 2016;81:153–61.
28. de Pablos-Martín A, Tismer S, Naumann F, Krause M, Lorenz M, Grundmann M, et al. Evaluation of the bond quality of laser-joined sapphire wafers using a fresnoite-glass sealant. Microsyst Technol. 2016;22:207–14.
29. Ashcom JB. The role of focusing in the interaction of femtosecond laser pulses with transparent materials. Cambridge, Massachusetts: Harvard University; 2003.
30. Kuryntsev S, Gilmutdinov AK. The effect of laser beam wobbling mode in welding process for structural steels. Int J Adv Manuf Technol. 2015;81(9-12):1683–91.
31. Data M, No S. Crofer 22 H material data sheet. No. 4050. 2010.
32. Lara C. Sellos vitrocerámicos del sistema RO-BaO-SiO_2 (R=Mg, Zn) para pilas de combustible de óxido sólido (SOFC). PhD Thesis: Universidad Autónoma de Madrid.2006.
33. Skarmoutsos D, Tietz F, Nikolopoulos P. Structure—property relationships of Ni/YSZ and Ni/(YSZ+TiO(2)) cermets. Fuel Cells. 2001;1(3–4):243–8.
34. Lara C, Pascual MJ, Durán A. Glass-forming ability, sinterability and thermal properties in the systems RO–BaO–SiO_2 (R=Mg, Zn). J Non-Cryst Solids. 2004;348:149–55.
35. Mahapatra MK, Lu K. Glass-based seals for solid oxide fuel and electrolyzer cells—A review. Mat Sci Eng R. 2010;67(5–6):65–85.
36. Meinhardt KD, Kim DS, Chou YS, Weil KS. Synthesis and properties of a barium aluminosilicate solid oxide fuel cell glass-ceramic sealant. J Power Sources. 2008;182(1):188–96.
37. Schwickert T, Sievering R, Geasee P, Conradt R. Glass-ceramic materials as sealants for SOFC applications. Materialwiss Werkst. 2002;33(6):363–6.
38. Jin T, Naylor MO, Shelby JE, Misture ST. Galliosilicate glasses for viscous sealants in solid oxide fuel cell stacks: Part III: behavior in air and humidified hydrogen. Int J Hydrogen Energ. 2013;38(36):16308–19.
39. Minh NQ, Takahashi T. Science and technology of ceramic fuel cellsElsevier Science 1995. ISBN: 9780080540764.
40. Blum L, Meulenberg WA, Nabielek H, Steinberger-Wilckens R. Worldwide SOFC technology overview and benchmark. Int J Appl Ceram Tec. 2005;2(6):482–92.
41. Jiang SP, Chan SH. A review of anode materials development in solid oxide fuel cells. J Mater Sci. 2004;39(14):4405–39.
42. Chou YS, Stevenson JW, Singh P. Effect of pre-oxidation and environmental aging on the seal strength of a novel high-temperature solid oxide fuel cell (SOFC) sealing glass with metallic interconnect. J Power Sources. 2008;184(1):238–44.
43. Chou YS, Stevenson JW, Singh P. Novel refractory alkaline earth silicate sealing glasses for planar solid oxide fuel cells. J Electrochem Soc. 2007;154(7):B644–B651.
44. Tulyaganov DU, Reddy AA, Kharton VV, Ferreira JMF. Aluminosilicate-based sealants for SOFCs and other electrochemical applications - A brief review. J Power Sources. 2013;242:486–502.
45. Kothiyal GP, Goswami M, Tiwari B, Sharma K, Ananthanarayanan A, Montagne L. Some recent studies on glass/glass-ceramics for use as sealants with special emphasis for high temperature applications. J Adv Ceram. 2012;1(2):110–29.
46. Fernández-Navarro,JM. El vidrio: Madrid, Editorial CSIC - CSIC Press, 2003
47. Volf MB. Mathematical Approach to Glass (Glass Science and Technology: Elsevier Science Publishers. Amsterdam: The Netherlands, 1988.
48. Pascual MJ, Duran A, Pascual L. Sintering process of glasses in the system Na_2O-B_2O_3-SiO_2. J Non-Cryst Solids. 2002;306(1):58–69.
49. Blanco B, Blaess C, Reinsch S, Brauer D, Müller R. Sintering and foaming of barium and calcium silicate glass powders. In:

Technologies M, editor. 11th Int Conf Exhib Ceram Interconnect Ceram Dresden. Germany, 2015; p. 31–7.
50. Rodríguez-López S, Haanappel V, Durán A, Muñoz F, Mather GC, Pascual MJ, et al. Glass ceramic seals in the system MgO-BaO-B_2O_3-SiO_2 operating under simulated SOFC conditions. Int J Hydrogen Energ. 2016;41(34):15335–45.
51. Rodríguez-López, S. Propiedades termo-mecánicas de sellos vitrocerámicos del sistema RO-MgO-B_2O_3-SiO_2 (R=Ba, Sr) para SOFCPhD Thesis: Universidad Autónoma de Madrid-Departamento de Física Aplicada. 2016.
52. Misture ST, Naylor MO, Jin T, Shelby JE. Galliosilicate glasses for viscous sealants in solid oxide fuel cell stacks: Part II: Interactions with yttria stabilized zirconia and stainless steel coated with alumina. Int J Hydrogen Energ. 2013;38(36):16328–37.
53. Rodríguez-López S, Wei J, Laurenti KC, Mathias I, Justo VM, Serbena FC, et al. Mechanical properties of solid oxide fuel cell glass-ceramic sealants in the system BaO/SrO-MgO-B2O3-SiO2. J Eur Ceram Soc. 2017;37(11):3579–94.
54. Wisniewski W, Döhler F, Rüssel C. Oriented nucleation and crystal growth of Ba-Fresnoite ($Ba_2TiSi_2O_8$) in 2BaO·TiO_2·2SiO_2 glasses with additional SiO_2. Cryst Growth Des. 2018;18(5):3202–8.
55. NagayamaK, UtsunomiyaY, KajiwaraT, PulseNT. Laser ablation by reflection of laser pulse at interface of transparent materials. In: Jakubczak E. Lasers - Applications in Science and Industry. IntechOpen. 2011.
56. Miralles V, Huerre A, Malloggi F, Jullien M-C. A review of heating and temperature control in microfluidic systems: techniques and applications. Diagnostics. 2013;3(1):33–67.

How to cite this article: de Pablos-Martín A, Rodríguez-López S, Pascual MJ. Processing technologies for sealing glasses and glass-ceramics. *Int J Appl Glass Sci*. 2020;00:1–17. https://doi.org/10.1111/ijag.15107